Available online at website: https://journal.bcrec.id/index.php/bcrec

Bulletin of Chemical Reaction Engineering & Catalysis, 20 (4) 2025, 650-660

Original Research Article

Enhancement of Charge Transfer in Quantum Dot–sensitized Solar Cell Photoanodes by Supporting rGO Layers

Dang Huu Phuc[1], Ha Thanh Tung[2*], Le Doan Duy[3,4,5], Le Minh Nhan[6]

[1]*Faculty of Fundamental Science, Industrial University of Ho Chi Minh City, Ho Chi Minh City, Viet Nam.*
[2]*Faculty of Basic Sciences, Vinh Long University of Technology Education, Vinh Long City, Vietnam.*
[3]*Faculty of Physics and Engineering Physics, VNUHCM-University of Science, Hochiminh City, Vietnam.*
[4]*Vietnam National University Hochiminh City, Hochiminh City, Vietnam.*
[5]*Faculty of Electrical & Electronics Engineering, Vinh Long University of Technology Education, Vinh Long Province, Vietnam.*
[6]*Department of Chemistry, Faculty of Basic Sciences, Can Tho University of Medicine and Pharmacy, Can Tho 94000, Vietnam.*

Received: 10th March 2025; Revised: 17th September 2025; Accepted: 18th September 2025
Available online: 24th September 2025; Published regularly: December 2025

Abstract

In this study, we have studied and fabricated quantum dot sensitized solar cells based on photoanodes with the support of rGO buffer layer to enhance the electron transfer ability from TiO_2 nano-semiconductor to FTO substrate. The rGO materials were fabricated by hydrothermal method, then they were coated on FTO substrate by Screen - Printing technique to create rGO nano films. The thickness of rGO films was studied from 1 to 3 layers to evaluate the mobility of charge, reduce recombination and resistance of film. Experimental results were determined by structural properties using XRD, FTIR, EDX and XPS, FESEM spectra; determined optical properties using UV-Vis absorption and transmission spectra; determined optical, electrical and chemical properties using Nyquist and EIS spectra. The maximum measured efficiency was 5.23% for the FTO/rGO(2)/TiO_2/QDs film, current density 21.34 mA/cm^2, open circuit voltage 5.525 V and fill factor of 0.34. These results were also proven through the research results of optical properties, electrochemical properties. In addition, these results are also consistent with the studies of others.

Keywords: rGO nanofilms; quantum dots; solar cells; charge transfer

How to Cite: Phuc, D.H., TTung, H.T., Duy, L.D., Nhan, L.M. (2025). Enhancement of Charge Transfer in Quantum Dot–sensitized Solar Cell Photoanodes by Supporting rGO Layers. *Bulletin of Chemical Reaction Engineering & Catalysis*, 20 (4), 650-660. (doi: 10.9767/bcrec.20366)

Permalink/DOI: https://doi.org/10.9767/bcrec.20366

1. Introduction

Renewable energy, especially solar energy, has gained significant attention due to fossil fuel depletion and environmental pollution [1–2]. Among solar conversion technologies, quantum dot-sensitized solar cells (QDSSCs) are considered promising because of their high theoretical power conversion efficiency (PCE), simple fabrication process, and low production cost [3–4]. A typical QDSSC is composed of an anode, a cathode, and a polysulfide electrolyte, in which the anode is crucial for photogenerated electron generation and transport, directly influencing device efficiency [5–6]. Titanium dioxide (TiO_2) has been extensively used as a photoanode material owing to its chemical stability, low cost, and environmental friendliness [7–8]. Various TiO_2 nanostructures (nanoparticles, nanotubes, nanosheets) have been explored to optimize electron transport and light harvesting. However, despite these efforts, the actual efficiency of QDSSCs remains much lower than the theoretical limit [9–11].

* Corresponding Author.
Email: tunght@vlute.edu.vn (H.T. Tung)

To address this limitation, researchers have proposed incorporating conductive carbon-based materials. Graphene and its derivatives, especially reduced graphene oxide (rGO), have shown potential due to their excellent electrical conductivity and high carrier mobility [12–13]. rGO can effectively improve electron transfer pathways and reduce recombination losses when integrated into semiconductor frameworks. Previous studies suggest that introducing rGO into TiO_2-based photoanodes enhances charge collection, yet challenges remain in establishing a stable conductive network within the TiO_2 layer [14–17].

Although rGO has been investigated as a conductive additive, limited studies have focused on employing it as an interfacial conductive layer to simultaneously repair TiO_2 structural cracks (formed during sintering) and enhance electron transport. Therefore, there is still a need for a practical strategy that integrates rGO into the TiO_2 framework in a way that both reinforces film integrity and improves conductivity.

This work aims to fabricate a novel FTO/rGO/TiO_2 photoanode for QDSSCs by introducing an rGO interlayer through a simple screen-printing method. The novelty of this design lies in the dual function of rGO: (i) bridging microcracks in the TiO_2 film and (ii) forming an effective conductive network. By accelerating photogenerated electron transfer, this approach is expected to significantly improve the photovoltaic performance of QDSSCs, thereby contributing to the advancement of cost-effective solar energy technologies.

2. Materials and Method

2.1 Materials

Graphene Oxide (GO) (Sigma Aldrich); Ethanol (Vietnam); Ethylene Glycol (Sigma Aldrich); Polyvinylpyrrolidone (PVP); Polyethylene Glycol (PEG) (Sigma Aldrich); Cadmium Acetate Dihydrate (China); Sodium Sulfide Nonahydrate (Sigma Aldrich); Selenium (Sigma Aldrich); Sodium Sulfite (China); Sodium Hydroxide (Sigma Aldrich); Zinc Nitrate Hexahydrate (China); Sulfur (China); Potassium Chloride (Sigma Aldrich); Copper(II) Chloride Dihydrate (China); Sodium Thiosulfate Pentahydrate (Sigma Aldrich); Copper(II) Sulfate Pentahydrate (Sigma Aldrich); Hydrochloric Acid (China); Methanol (Thailand); TiO_2 Paste Transparent 18NR-T (Australia). All materials have a purity of 99.9% and are used for analytical purposes.

2.2 Synthesis of FTO/rGO/TiO_2 Photoanodes

24 mg GO was ultrasonically processed in a solution of 30 mL ethanol and ethylene glycol for 1 hour. After that, the mixture was put into teflon, and hydrothermally heated at 180 ℃ for 24 hours. The mixture had a dark blue color after hydrothermal treatment. The mixture of washing solution was mixed in a ratio of ethanol: distilled water (1:3) and centrifuged to get the solid. After completely removing the washing water, the solid was dried at 60 ℃ for 12 hours. After drying, the solid was ground into a fine powder and mixed with a mixture of 10 mL ethanol and 0.25 g PEG (Polyethylene glycol) to create a gel with a certain viscosity. rGO paste was attached to FTO glass by the doctor blade method with different number of scans, and the sample was labeled FTO/rGO film. FTO/rGO film was baked at 350 ℃ for 30 minutes. FTO/rGOd-layer/TiO_2 electrode was fabricated by depositing TiO_2 layer on FTO/rGOd-layer glass deposited by Screen - Printing method, then calcined at 500 °C for 30 min.

2.3 Fabrication of FTO/rGO/TiO_2/CdS/CdSe:Cu^{2+}(0.3%)/ZnS Photoanodes

CdS, CdSe:Cu^{2+}(0.3%), and ZnS layers were deposited on the FTO/rGO/TiO_2 film by SILAR method. The FTO/rGO/TiO_2 photoanode was immersed in a solution containing Cd^{2+} ions (0.1 M) for 5 min and washed with ethanol. The electrode was further immersed in a solution containing S^{2-} ions (0.1 M) for 5 min and then washed with methanol, the process was repeated for 3 SILAR cycles. The photoanode was dried for 15 min at 120 ℃. The CdSe:Cu^{2+}(0.3%) layer was deposited on the FTO/rGO/TiO_2/CdS electrode using the same process as the CdS layer. The prepared solutions were Cd^{2+} and Cu^{2+} ions (0.1 M), ethanol washing solution, Se^{2-} ions (0.3 M), and distilled water washing solution, respectively.

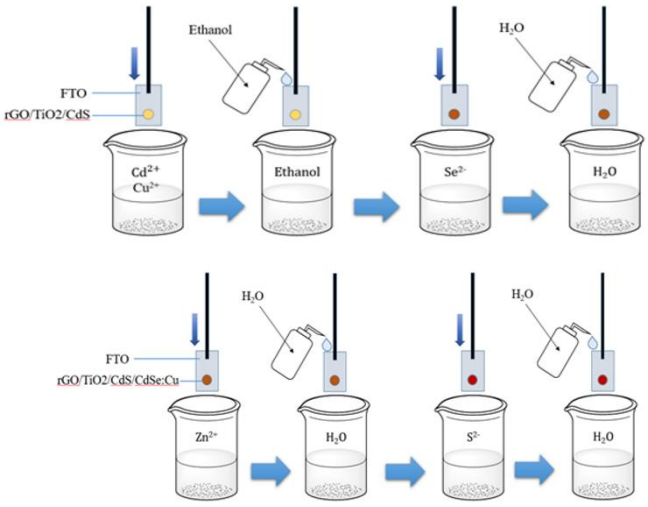

Figure 1. Schematic diagram of the synthesis and deposition process of ZnS nanocrystals onto FTO/TiO_2/CdS/CdSe:Cu^{2+} by SILAR method.

The ZnS surface protection layer was prepared with Zn^{2+} ions (0.1 M), distilled water washing solution, S^{2-} ions (0.1 M), and distilled water washing solution with 2 SILAR cycles (Figure 1).

2.4 Preparation of FTO/Cu_2S Cathodes

The Cu_2S layer was deposited on FTO glass by chemical bath deposition method, in a mixture of Cu^{2+} and S^{2-} under N_2 atmosphere, in an oil bath for 30 min at 90 ℃. Then, the FTO/Cu_2S film was rinsed with distilled water, and the glass was dried for 30 min at 200 ℃.

2.5 Polysultfide Electrolyte

The electrolyte solution is a polysulfide with the redox couple S^{2-}/S_n^{2-} synthesized by dissolving 1.2 g Na_2S with 0.064 g S powder and 0.149 g KCl with corresponding concentrations (0.5 M, 0.2 M, 0.2 M) in 10 mL of a mixture of distilled water:methanol solution with a ratio of 7:3.

2.6 Processes of Completed QDSSCs

QDSSC solar cells were assembled between FTO/rGO/TiO_2/CdS/CdSe:Cu^{2+}(0.3%)/ZnS films and FTO/Cu_2S cathode by surlyn with size of 1.2 x 1 cm, with surlyn bonding temperature at 200 ℃ for 10 s (Figure 2).

3. Results and Discussion

The structures of rGO/TiO_2:GO, FTO/rGO, and FTO/rGO/TiO_2 films with different numbers of rGO layers were measured by FTIR spectroscopy, the results are shown in Figure 3. The FTIR spectrum of FTO/TiO_2 films contains characteristic vibrational peaks for Ti–O–Ti groups at 518 and 636 cm^{-1}, 465 cm^{-1} and finally at 974 cm^{-1} and 1627 cm^{-1} are characteristic peaks for O–Ti–O and Ti–OH groups, respectively. For GO films, there is a strong broad peak at 3400 cm^{-1}, indicating the presence of characteristic vibrational peak for -OH groups in GO samples. In addition, the vibration peak of the FTO/rGO/TiO_2 composite material appeared [18] with small peaks at 1710 cm^{-1} characteristic of the carbonyl group (C=O) of carboxylic acid. The peak at 1625 cm^{-1} represents the -OH bending vibration and the C=C stretching vibration and finally the characteristic peak for the C-O group at 1060 cm^{-1} [18,19]. The FTIR spectrum of the FTO/rGO membrane has peaks at about 2330, 1821, 1532 and 1119 cm^{-1} corresponding to the functional groups C–H, C=O, C=C and C–OH, respectively [20]. The result of the successful reduction of GO to rGO is clearly shown in the decrease of the functional groups containing oxygen (O-H) [21-23]. The FTIR spectrum of the FTO/rGO/TiO_2 structured material showed the combination of vibrational peaks of rGO and TiO_2, thereby indicating that rGO and TiO_2 were successfully combined. The transmission spectra of different samples, including rGO/TiO_2:GO (black), FTO/rGO (red), FTO/TiO_2 (green),

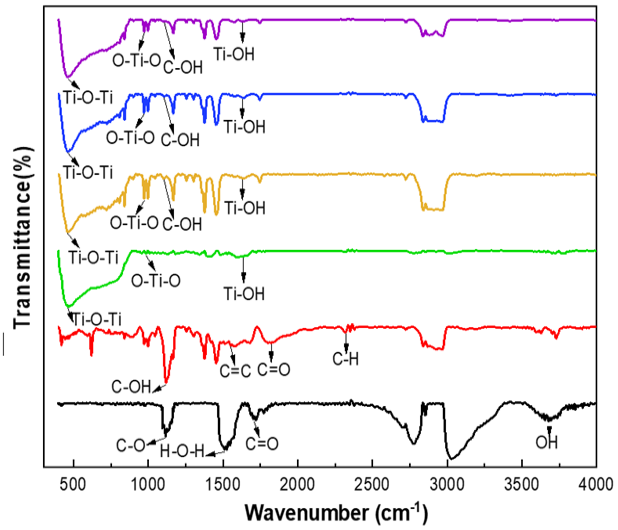

Figure 3. FTIR of rGO/TiO_2:GO (black); FTO/rGO(red); FTO/TiO_2 (green); FTO/rGO(1)/TiO_2 (yellow) ; FTO/rGO(2)/TiO_2 (blue); FTO/rGO(3)/TiO_2 (violet).

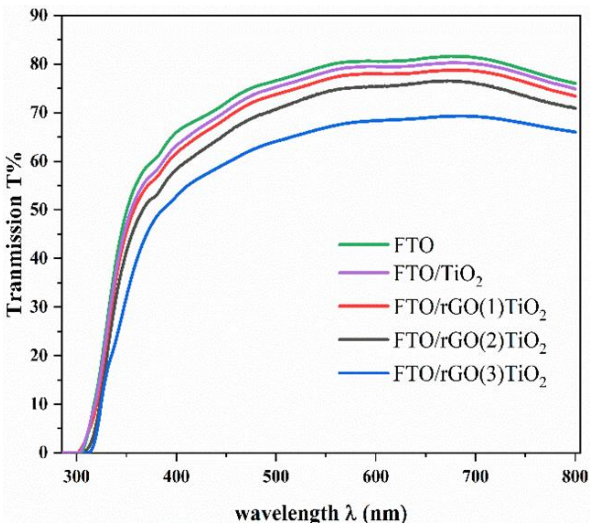

Figure 4. Transmission of rGO/TiO_2:GO (black), FTO/rGO(red), FTO/TiO_2 (green), FTO/rGO(1)/TiO_2 (yellow), FTO/rGO(2)/TiO_2 (blue), FTO/rGO(3)/TiO_2 (violet).

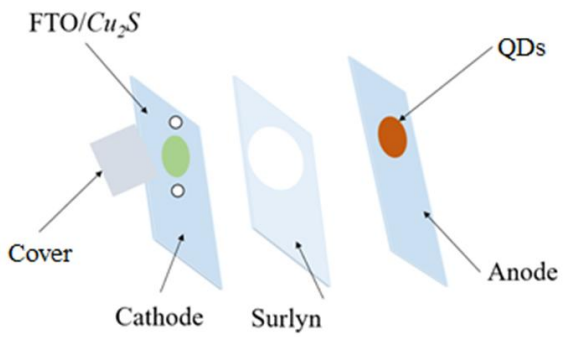

Figure 2. Assembly process of a completed QDSSCs.

FTO/rGO(1)/TiO_2 (yellow), FTO/rGO(2)/TiO_2 (blue), and FTO/rGO(3)/TiO_2 (violet), were measured in Figure 4. All samples exhibited transmittance values exceeding 70% in the visible region above 400 nm.

XRD patterns of TiO_2 materials and the composite materials of TiO_2 and rGO on FTO substrate are shown in Figure 5. From these patterns, the results of FTO materials on the anatase TiO_2 structure were determined through the peaks appearing at 25.74°, 48.4°, 55.01°, 65.8° of the anatase TiO_2 phase, corresponding to their lattice planes (101), (200), (211) and (116). Besides, no peaks related to rGO or carbon were found in the X-ray diffraction patterns likely due to the layers of rGO are much thinner than the TiO_2 layers [24-25].

Raman spectroscopy is a non-destructive technique to study the various non-polar vibrational bonds present in the crystal structure. The changes in the oxygen groups in GO during the hydrothermal process can also be explained using this spectroscopic technique. Figure 6 shows the Raman spectra of FTO/TiO_2, FTO/rGO, FTO/rGO(1)/TiO_2, FTO/rGO(2)/TiO_2, FTO/rGO(3)/TiO_2 films. The results show that the reduced graphene oxide (rGO) exhibits Raman peaks at the wavenumber positions of 1350 cm^{-1} and 1595 cm^{-1}. The peak positions of 1350 cm^{-1} and 1595 cm^{-1} are identified as the internal structural defects of sp2 carbon (D band) and the well-ordered phonon vibrations inside the sp2 bonded carbon atoms (G band), respectively. The vibrational features related to the 2D band of graphene were observed at 2645 cm^{-1} [18]. The anatase TiO_2 phase has vibrational features E_g, B_{1g}, B_{1g} + A_{1g} and E_g observed at wavenumbers 154, 400, 515 and 640 cm^{-1}. The average ratio between the intensity of the D and G bands (ID/IG) for the composites prepared here was less than 1 (Table 1). The results showed that the rGO layered structure had high crystallinity and few defects.

The surface morphology of the FTO samples coated with rGO from 1 to 3 layers is shown in Figure 7. Starting from two layers of rGO, the surface morphology of rGO was initially formed on the FTO layers. However, under these conditions, some areas were not completely covered by rGO as observed in Figure 7a. As the number of rGO layers increased, the surface morphology became uniform, in FTO/ rGO(2) the number of uncovered sites decreased as observed in Figure 7b. The surface morphology of FTO/ rGO(3) was much rougher than that of FTO/ rGO(2), as evidenced by the multiple rGO layers stacked on top of each other.

In addition, the surface morphology of rGO/TiO_2 was observed to be consisten across all samples had similar morphology indicating the natural porous structure of TiO_2. This suggests that, the rGO/TiO_2 layers retained their porosity, which would be advantageous for the retention of QDs during the silane process at a later stage. The rGO/TiO_2 samples were then used to fabricate CdS QDSSCs. Generally, the fabricated QDs were smaller than 10 nm in size, as reported in a previous study [26]. Thus, there would not be any significant morphology differences was observed

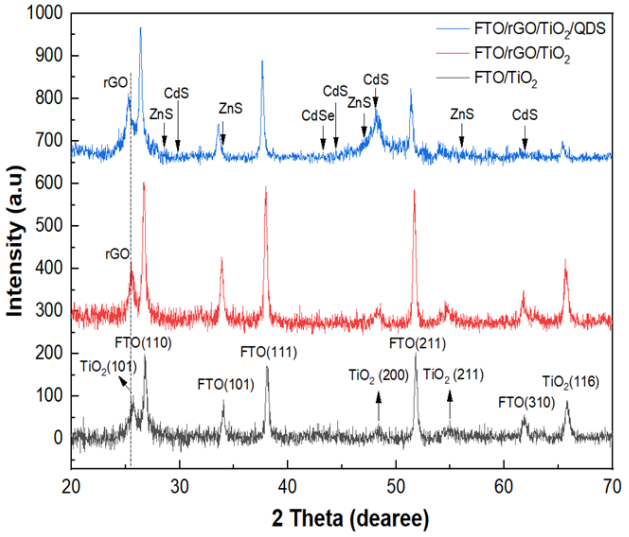

Figure 5. The XRD of rGO/TiO_2, FTO/TiO_2 (orange), FTO/rGO/TiO_2 (green).

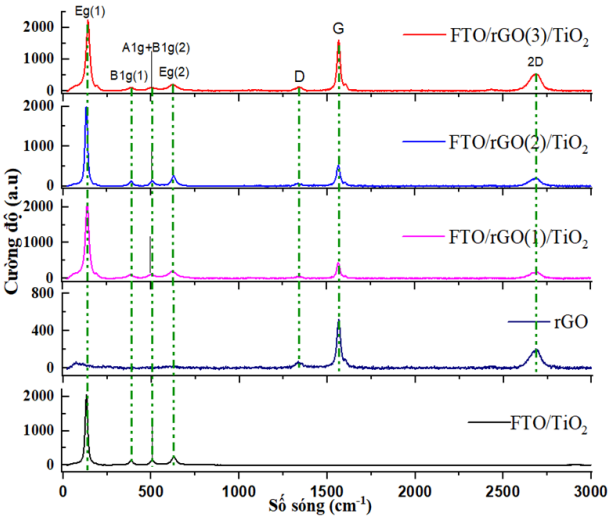

Figure 6. The Raman of FTO/rGO/TiO_2 photoanode.

Table 1. Intensity of D, G and D/G peaks.

Samples	D	G	D/G
rGO	8.7	527.4	0.15
FTO/rGO (1)/TiO_2	65.4	459.2	0.14
FTO/rGO (2)/TiO_2	74.6	535.1	0.13
FTO/rGO (3)/TiO_2	134.5	1612.9	0.08

under FESEM because of the small size of the fabricated QDs.

An energy-dispersive X-ray spectroscopy analysis was investigated the chemical composition and the formation of the synthesized FTO/rGO(3)/TiO_2 layer with the results illustrated in Figure 8d and Table 2. The EDX spectral results have successfully confirmed the fabrication of the FTO/rGO(3)/TiO_2 structure. The results indicated the presence of characteristic peaks of Ti at 3.0 eV, 4.2 eV, and 5.1 eV; for Oxygen (O) at 0.2 eV, and for carbon (C) at 0.4 eV [27]. Moreover, the peaks were of high intensity, narrow widths and sharp half profiles, which confirmed the crystalline nature of the FTO/rGO(3)/TiO_2 composites.

Figure 9 presents the XPS spectra of FTO/rGO/TiO_2 and FTO/TiO_2 anodes, revealing characteristic peaks of C1s, Ti2p, and O1s (Figure 9a) [28-29]. Ti2p1/2 and Ti2p3/2 peaks appear at 465.1 eV and 459.1 eV, respectively, with no significant difference in intensity (Figure 9b). The O1s spectra (Figure 9c, 9d) indicate oxygen vacancies (OV) at 531.3 eV, OO-H at 532.9 eV, and OO-Ti at 530.2 eV in FTO/rGO/TiO_2. The stronger oxygen-related signal in FTO/TiO_2 suggests incomplete reduction of GO to rGO during calcination at 500 °C [30].

The C1s spectra (Figures 9e, 9f) exhibit peaks at 284.6 eV (C–C), 286.2 eV (C=O), and 288.8 eV (C–O), with FTO/rGO/TiO_2 showing higher intensity. The proportion of C–OH, C–O–C, C=O,

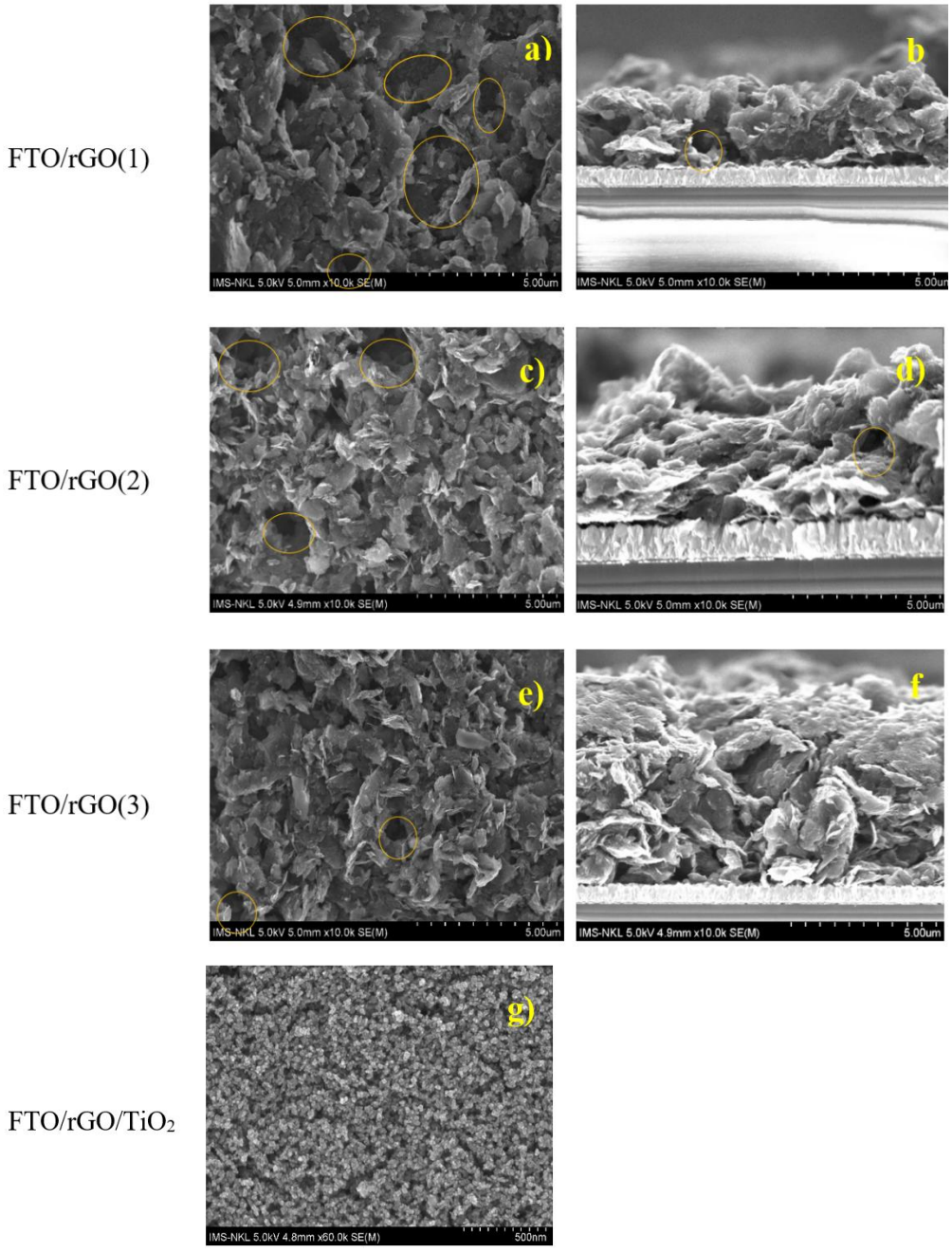

Figure 7. The FESEM of (a) FTO/rGO(1), (c) FTO/rGO(2), (e) FTO/rGO(3), and (g) FTO/rGO/TiO_2. Cross – section FESEM of (b) FTO/rGO(1), (d) FTO/rGO(2), and (f) FTO/rGO(3).

and COOH bonds reflects the degree of deoxygenation. The sp^2 (C=C) and sp^3 (C–C) species appear at 284.2 eV and 285 eV, respectively [31-32]. Increased C=C bonds in irradiated samples confirm rGO formation. Additionally, a peak at 282 eV suggests Ti–C bond formation, indicating chemical interaction between carbon and TiO_2 [33]. Oxidation of carbon groups (C–OH, C–O–C, C=O, O=C–OH) is observed at higher binding energies (286.0–290.0 eV).

The photovoltaic performance of QDSSCs based on FTO/rGO(0-3)/TiO_2 composite was investigated by current density-voltage characterization (Keithley 2450 spectrophotometer - AM1.5, 100 mW/cm^2). The J–V diagrams were reported in Figure 10, where the active area of each sample is 0.168 cm^2. The parameters are presented in Table 3. The sample without rGO had the lowest efficiency of 4.52% with a photocurrent density of 22.65 mA/cm^2. In addition, the efficiency of QDSSCs was increased when the TiO_2 photoanode was layered with a small amount of rGO. The short-circuit photocurrent (J_{SC}) densities of QDSSCs based on FTO/TiO_2, FTO/rGO/TiO_2 (d = 1, 2, 3) were 22.65, 27.42, 21.34, and 20.97 mA/cm^2. The results showed that the addition of rGO layer between the FTO and TiO_2 layers would help improve the energy band alignment, leading to better charge transfer. This sample produced better current density and open-circuit voltage, which was further reflected in the fill factor (FF) value. The presence of rGO would facilitate the charging and charge moving in films. Moreover, rGO also helped to broaden the spectral light absorption range [34]. In this case, rGO could act as an electron acceptor from TiO_2 and quantum dots; thus, reducing electron-hole pair recombination. In addition, the decrease in current density with increasing number of rGO layers may be due to the decrease in visible light transmission, which will affect the conversion efficiency of the solar cell. In contrast, the open circuit potential

Table 2. Atomic percentage of FTO/rGO/TiO_2.

Sample	C	O	Ti
Weight%	1.37	44.57	54.07
Atomic%	2.82	69.16	28.02

Table 3. Parameters of FTO/rGO(d)/TiO_2/QDs with various layers of rGO.

Photoanodes	J_{sc}	V_{oc}	*FF*	η(%)
FTO/TiO_2/QDs	22.65	0.5	0.4	4.52
FTO/rGO(1)/TiO_2/QDs	27.42	0.52	0.44	4.84
FTO/rGO(2)/TiO_2/QDs	21.34	0.525	0.47	5.23
FTO/rGO(3)/TiO_2/QDs	20.97	0.54	0.45	5.14

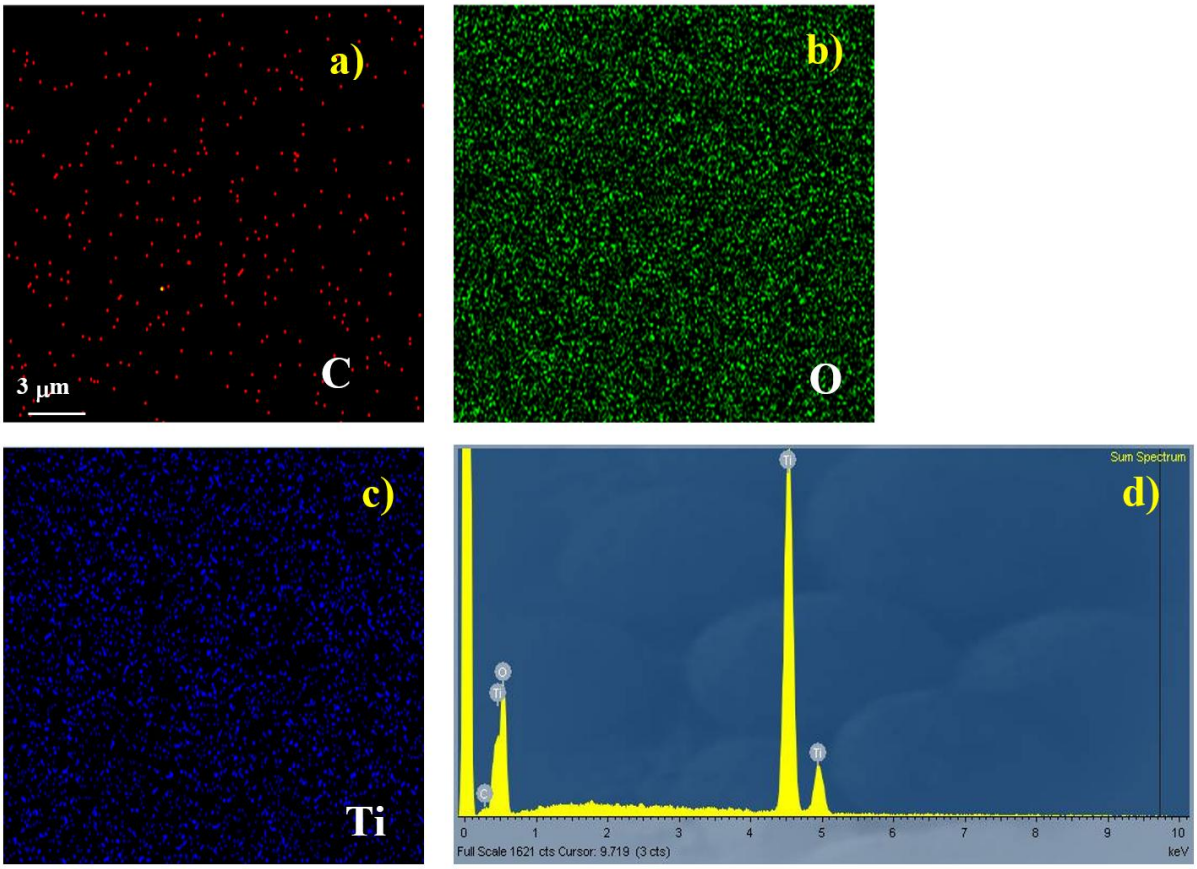

Figure 8. (a-c) Image elements of FTO/rGO/TiO_2, and (d) the EDX spectrum of FTO/rGO/TiO_2.

enhanced from 0.5 V (FTO/TiO_2) to 0.525 V (rGO(2)/TiO_2), and then reached 0.54 V for (rGO(3)/TiO_2). The change of FF was similar to that of V_{OC}. The results showed that the power conversion efficiency (η(%)) of QDSSC reached 5.23% at the optimal number of rGO layers of 2. The results showed that the rGO layer with TiO_2 improved the bonding between TiO_2 and FTO, leading to better electron transfer and contributing to the prevention of electron-hole pair recombination [35,36]. To elucidate the charge kinetics effect of rGO/TiO_2 composite film, the QDSSCs were analyzed by EIS. The measurements were carried out in the dark at open circuit voltage. In this work, the fabricated QDSSC based on the FTO/rGO(2)/TiO_2 photoanode achieved a power conversion efficiency (PCE) of 5.23%. Compared with previous reports on QDSSCs using rGO-modified TiO_2 photoanodes, which typically show efficiencies in the range of 3–5% [35,36], our result is at the higher end of this range. This indicates that the dual rGO interlayer strategy is an effective approach to further enhance electron transport and reduce recombination losses. The improvement highlights the novelty of our method in constructing a more continuous conductive network between TiO_2 and QDs, leading to better device performance.

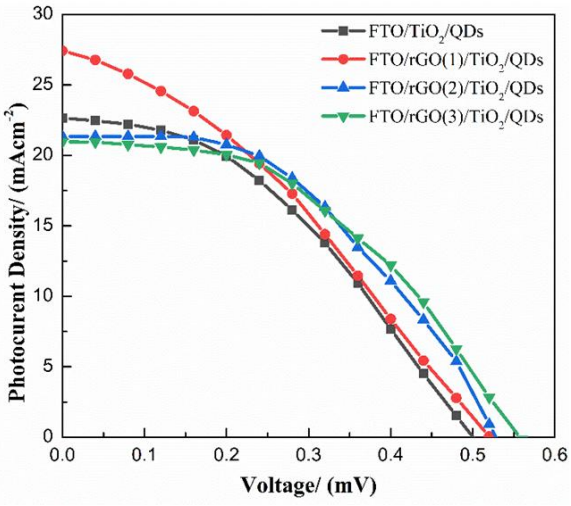

Figure 10. The J-V of QDSSCs with various layers of rGO.

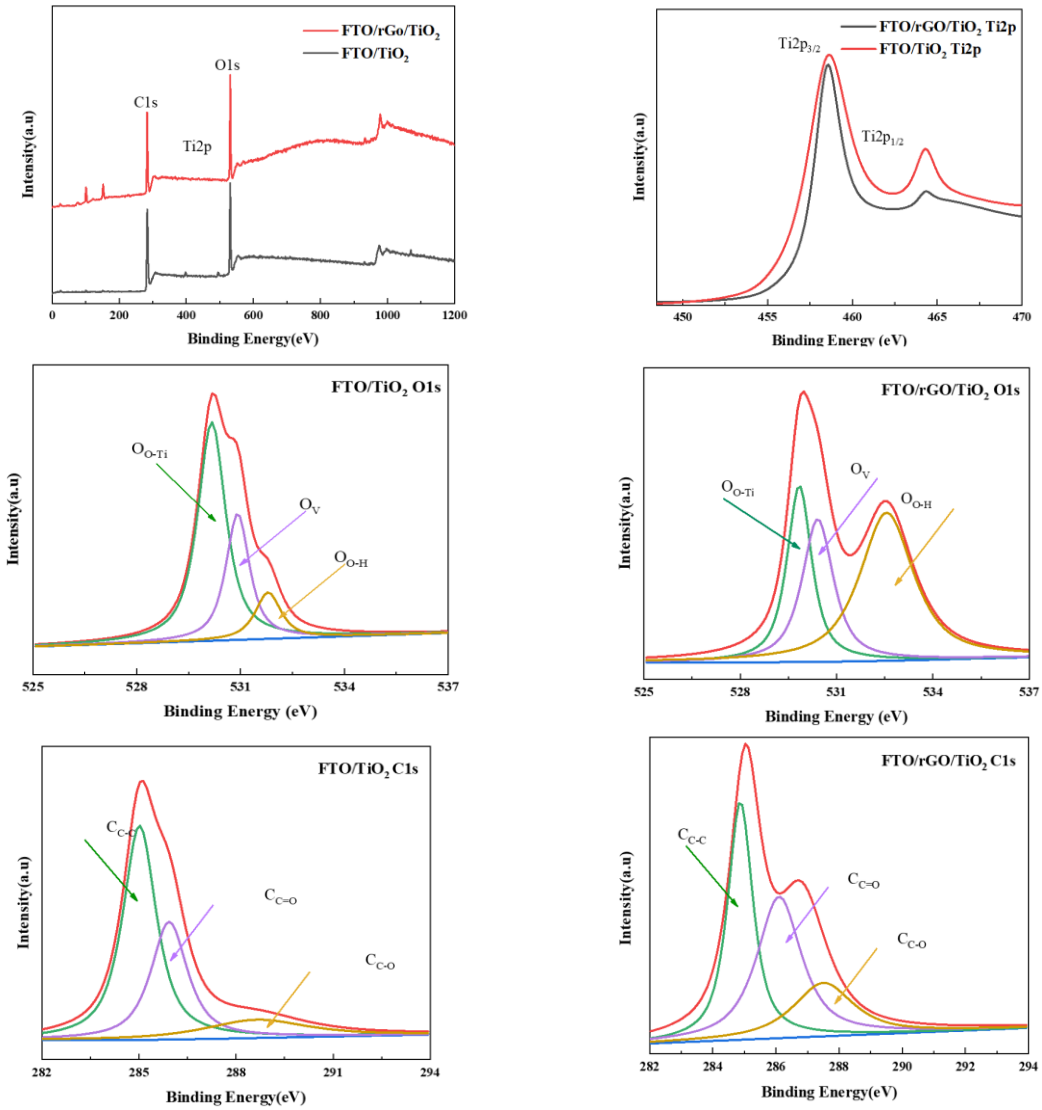

Figure 9. The XPS of FTO/rGO/TiO_2 and FTO/TiO_2 photoanodes.

The Nyquist plot provides insights into the electron migration kinetics in different QDSSCs structures. Figure 11 presents the Nyquist plot of each QDSSCs, fitted using the equivalent circuit shown in the inset, which consists of three components [25]. The series resistance (R_s) in the high-frequency region reflects the resistances of the electrolyte, electrode, and FTO layer. The charge transfer resistance (R_{ct}) at the electrolyte/counter electrode interface and the constant phase element (CPE) representing the electric double-layer capacitor dominate the mid-frequency region [26]. In the low-frequency region, Rct corresponds to charge transfer resistance at the TiO_2/QD or rGO/TiO_2/QDs interface, while CPE represents capacitance.

The R_s values (Table 4) remained consistent across samples, confirming that the rGO layer did not enhance the anode electrode film's resistance. The R_{ct} of QDSSCs incorporating rGO remained largely unchanged due to the use of the same CuS anode, and polysulfide. But, cell with rGO exhibited significantly lower R_{ct} than the TiO_2-only structure, demonstrating enhanced charge transfer at the rGO/TiO_2 and QDs interface. This reduction in charge transfer resistance highlights the rGO layer's role in facilitating electron transport. The lower resistance observed in the photoanode with two rGO layers can be attributed to the formation of a more continuous and efficient conductive network. With a single rGO layer, the coverage may be incomplete, leaving localized regions of high resistance due to cracks or grain boundaries in the TiO_2 film. By introducing two rGO layers, these defects are more effectively bridged, and multiple conductive pathways are established, which facilitates faster electron transport and reduces charge recombination. Therefore, the dual-layer structure minimizes interfacial resistance between TiO_2 and QDs, leading to the lowest overall resistance and improved photovoltaic performance.

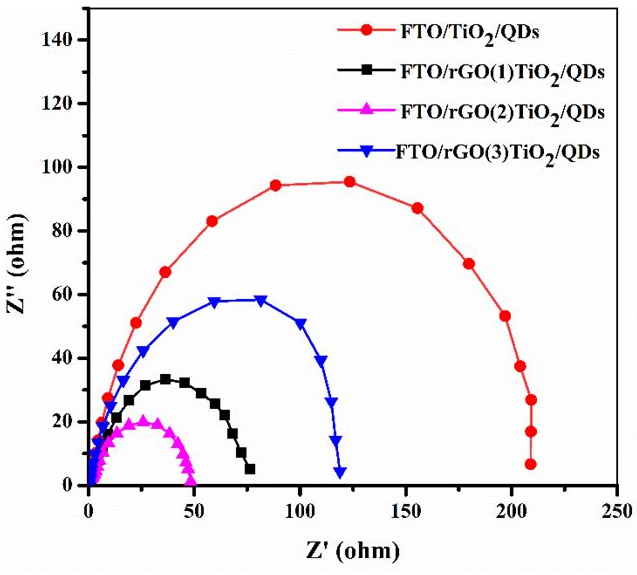

Figure 11. The Nyquist of QDSSCs

Figure 12 illustrates the structure of a quantum dot solar cell consisting of the photoanode, cathode, and electrolyte components. This section focus on the energy band structure of the photoanode. When the photoanode film is illuminated, the CdS, CdSe, and ZnS quantum dots absorb photons, generating electrons in their conduction bands. These electrons subsequently move through the conduction band of the TiO_2 film to the external circuit. For photoanode films without rGO support, electron loss occurs due to recombination in surface trap states. However, for photoanodes with rGO support, electrons are transferred more efficiently, thereby reducing the loss due to recombination.

4. Conclusions

Quantum dot sensitized solar cells using photoanodes with FTO/rGO/TiO_2/QDs structure have been successfully fabricated. In the FTO/rGO/TiO_2/QDs structure, rGO is used as a buffer layer to support the charge transfer process between QDs, TiO_2, and FTO. QDSSCs with FTO/rGO(2)/TiO_2/QDs photoanode achieved the highest photoelectric conversion efficiency of 5.23%. In general, all FTO/rGO(1-3)/TiO_2/QDs photoanodes have higher efficiency than photoanodes without rGO layer support. This demonstates the effective support of rGO layer in the electron transfer process through the contact layers. This result is also proven by the analysis of electrochemical impedance spectrum. The curve-fitting result shows that of the resistance of photoanode with two rGO layers is the lowest. This result shows that the flexibility as well as the conductivity of rGO membranes have increased under our fabrication conditions.

Acknowledgment

The authors wish to express the colleagues for providing the resources and support needed to complete this study.

Table 4. The EIS characteristics were estimated from the Nyquist plots of the symmetrical cells for FTO/rGO/TiO_2/QDs CEs.

Samples	R_S (Ω)	R_{ct} (Ω)	C_{PE} (μF)
FTO/TiO2/QDs	38.05	278.5	0.90
FTO/rGO(1)/TiO_2/QDs	33.19	120.5	0.92
FTO/rGO(2)/TiO_2/QDs	25.08	61.9	0.87
FTO/rGO(3)/TiO_2/QDs	31.19	81.5	0.92

CRedit Author Statement

Author Contributions: Dang Huu Phuc: Writing Draft Preparation, Visualization, Resources, Methodology, Formal Analysis; Ha Thanh Tung: Methodology, Formal Analysis, Data Curation, Review and Editing; Le Doan Duy, Le Minh Nhan: Methodology, Investigation. All authors have read and agreed to the published version of the manuscript.

References

[1] Zaban, A., Mićić, O.I., Gregg, B.A., Nozik, A.J. (1998). Photosensitization of nanoporous TiO_2 electrodes with InP quantum dots. *Langmuir*, 14(12), 3153–3156. DOI: 10.1021/la9713863.

[2] Yu, P., Zhu, K., Norman, A., Ferrere, S., Frank, A., Nozik, A. (2006). Nanocrystalline TiO_2 solar cells sensitized with InAs quantum dots. *Journal of Physical Chemistry B*, 110(50), 25451–25454. DOI: 10.1021/jp064817b.

[3] Yu, W.W., Qu, L., Guo, W., Peng, X. (2003). Experimental determination of the extinction coefficient of CdTe, CdSe, and CdS nanocrystals. *Chemistry of Materials*, 15(14), 2854–2860. DOI: 10.1021/cm034081k.

[4] Beard, M.C. (2011). Multiple exciton generation in semiconductor quantum dots. *Journal of Physical Chemistry Letters*, 2(11), 1282–1288. DOI: 10.1021/jz200166y.

[5] Fang, J., Wu, J., Lu, X., Shen, Y., Lu, Z. (1997). Sensitization of nanocrystalline TiO_2 electrode with quantum-sized CdSe and ZnTCPc molecules. *Chemistry Letters*, 270(1-2), 145–151. DOI: 10.1016/S0009-2614(97)00333-3.

[6] Lee, W., Kwak, W.-C., Min, S.-K.; Lee, J.-C.; Chae, W.-S.; Sung, Y.-M.; Han, S.-H. (2008). Spectral broadening in quantum dots-sensitized photoelectrochemical solar cells based on CdSe and Mg-doped CdSe nanocrystals. *Electrochemistry Communications*, 10(11), 1699-1702. DOI: 10.1016/j.elecom.2008.08.025.

[7] Liu, D., Kamat, P.V. (1993). Photoelectrochemical behavior of thin cadmium selenide and coupled TiO_2/CdSe semiconductor films. *The Journal of Physical Chemistry*, 97(41), 10769-10773. DOI: 10.1021/j100143a041.

[8] Peter, L.M., Riley, D.J., Tull, E.J., Wijayantha, K.G.U. (2002). Photosensitization of nanocrystalline TiO_2 by self-assembled layers of CdS quantum dots. *Chemical Communications*, (10), 1030-1031. DOI: 10.1039/B201661C.

[9] Vogel, R., Pohl, K., Weller, H. (1990). Sensitization of highly porous, polycrystalline TiO_2 electrodes by quantum-sized CdS. *Chemical Physics Letters*, 174(3-4), 241-246. DOI: 10.1016/0009-2614(90)85339-E.

[10] Mora-Seró, I., Giménez, S., Moehl, T., Fabregat-Santiago, F., Lana-Villareal, T., Gómez, R., Bisquert, J. (2008). Factors determining the photovoltaic performance of a CdSe quantum dot sensitized solar cell: the role of the linker molecule and of the counter electrode. *Nanotechnology*, 19(42), 424007. DOI: 10.1088/0957-4484/19/42/424007.

[11] Shen, Y.-J., Lee, Y.-L. (2008). Assembly of CdS quantum dots onto mesoscopic TiO_2 films for quantum dot-sensitized solar cell applications. *Nanotechnology*, 19(4), 045602. DOI: 10.1088/0957-4484/19/04/045602.

[12] Lee, Y.-L.; Lo, Y.-S. (2009). Highly efficient quantum-dot-sensitized solar cell based on co-sensitization of CdS/CdSe. *Advanced Functional Materials*, 19(4), 604-609. DOI: 10.1002/adfm.200800940.

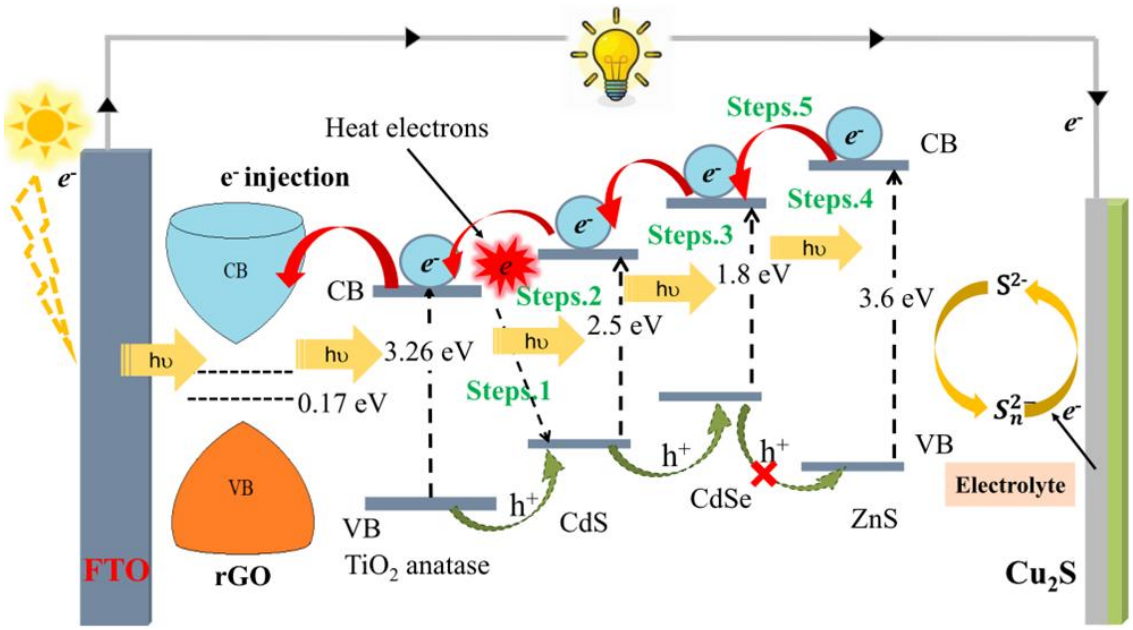

Figure 12. The structure of QDSSCs.

[13] Zhang, Q., Zhang, Y., Huang, S., Huang, X., Luo, Y., Meng, Q., Li, D. (2010). Application of carbon counterelectrode on CdS quantum dot-sensitized solar cells (QDSSCs). *Electrochemistry Communications*, 12(2), 327-330. DOI: 10.1016/j.elecom.2009.12.032.

[14] Sudhagar, P., Jung, J.-H., Park, S., Lee, Y.-G., Sathyamoorthy, R., Kang, Y.-S., Ahn, H. (2009). The performance of coupled (CdS:CdSe) quantum dot-sensitized TiO_2 nanofibrous solar cells. *Electrochemistry Communications*, 11(11), 2220-2224. DOI: 10.1016/j.elecom.2009.09.035.

[15] Yu, Z., Zhang, Q., Qin, D., Luo, Y., Li, D., Shen, Q., Toyoda, T., Meng, Q. (2010). Highly efficient quasi-solid-state quantum-dot-sensitized solar cell based on hydrogel electrolytes. *Electrochemistry Communications*, 12(12), 1776-1779. DOI: 10.1016/j.elecom.2010.10.022.

[16] Wang, S., Tian, J. (2016). Recent advances in counter electrodes of quantum dot-sensitized solar cells. *RSC Adv.* **6**(93), 90082-90099. DOI: 10.1039/C6RA19226B.

[17] Kamaja, C.K., Devarapalli, R.R., Dave, Y., Debgupta, J., Shelke, M.V. (2016). Synthesis of novel Cu_2S nanohusks as high performance counter electrode for CdS/CdSe sensitized solar cell. *J. Power Sources* 315, 277-283. DOI: 10.1016/j.jpowsour.2016.03.027.

[18] Tachan, Z., Shalom, M., Hod, I., Rühle, S., Tirosh, S., Zaban, A. (2011). PbS as a highly catalytic counter electrode for polysulfide-based quantum dot solar cells. *J. Phys. Chem. C* 115(13), 6162-6166. DOI: 10.1021/jp112010m.

[19] Kim, H.-J., Kim, D.-J., Rao, S.S., Savariraj, A.D., Kim, S.-K., Son, M.-K., Gopi, C.V.V.M., Prabakar, K.J.E.A. (2014). Highly efficient solution processed nanorice structured NiS counter electrode for quantum dot sensitized solar cells. *Electrochimica Acta,* 127, 427-432. DOI: 10.1016/j.electacta.2014.02.019.

[20] Chen, H., Zhu, L., Liu, H., Li, W. (2014). Efficient iron sulfide counter electrode for quantum dots-sensitized solar cells. *J. Power Sources,* 245, 406-410. DOI: 10.1016/j.jpowsour.2013.06.004.

[21] Raj, C.J., Prabakar, K., Savariraj, A.D., Kim, H.J. (2013). Surface reinforced platinum counter electrode for quantum dots sensitized solar cells. *Electrochimica Acta*, 103, 231-236. DOI: 10.1016/j.electacta.2013.04.016.

[22] Selopal, G.S., Zhao, H., Tong, X., Benetti, D., Navarro-Pardo, F., Zhou, Y., Barba, D., Vidal, F., Wang, Z.M., Rosei, F. (2017). Highly stable colloidal "giant" quantum dots sensitized solar cells. *Advanced Functional Materials*, 27(30), 1701468. DOI: 10.1002/adfm.201701468.

[23] Jiao, S., Shen, Q., Mora-Seró, I., Wang, J., Pan, Z., Zhao, K., Kuga, Y., Zhong, X., Bisquert, J. (2015). Band engineering in core/shell ZnTe/CdSe for photovoltage and efficiency enhancement in exciplex quantum dot sensitized solar cells. *ACS Nano*, 9(1), 908-915. DOI: 10.1021/nn506638n.

[24] Kim, J.-Y., Yang, J., Yu, J. H., Baek, W., Lee, C.-H., Son, H.J., Hyeon, T., Ko, M.J. (2015). Highly efficient copper–indium–selenide quantum dot solar cells: suppression of carrier recombination by controlled ZnS overlayers. *ACS Nano*, 9(11), 11286-11295. DOI: 10.1021/acsnano.5b04917.

[25] Youn, D.H., Kim, H.-S., Kang, H.-W., Park, C.-P., Huh, S., Park, J.-H., Lee, J., Lee, J. (2013). TiN nanoparticles on CNT–Graphene hybrid support as noble-metal-free counter electrode for quantum-dot-sensitized solar cells. *ChemSusChem*, 6(2), 261-267. DOI: 10.1002/cssc.201200775.

[26] Dao, V.-D., Choi, Y., Yong, K., Lee, J., Kim, M., Song, J. (2015). Graphene-based nanohybrid materials as the counter electrode for highly efficient quantum-dot-sensitized solar cells. *Carbon*, 84, 383-389. DOI: 10.1016/j.carbon.2014.12.067.

[27] Bae, G., Han, S., Kim, J. Y., Jang, J.-W., Park, ., Choi, S. H., Lee, J. S. (2013). A highly efficient transition metal nitride-based electrocatalyst for oxygen reduction reaction: TiN on a CNT–graphene hybrid support. *Journal of Materials Chemistry A*, 1(27), 8007-8015. DOI: 10.1039/C3TA11135K.

[28] Geim, A., Novoselov, K. (2010). *Nanoscience and Technology: A Collection of Reviews from Nature Journals*, edited by P. Rodgers. 2010, Singapore: World Scientific.

[29] Roy-Mayhew, J.D., Bozym, D.J., Punckt, C., Aksay, I.A. (2010). Functionalized graphene as a catalytic counter electrode in dye-sensitized solar cells. *ACS Nano*, 4(10), 6203-6211. DOI: 10.1021/nn1016428.

[30] Shi, M., Du, X., Zhang, Y., Ye, Z., Yang, D. (2012). Preparation of graphene–TiO_2 composite by hydrothermal method from peroxotitanium acid and its photocatalytic properties. *Applied Catalysis B: Environmental*, 405, 30-37. DOI: 10.1016/j.colsurfa.2012.04.031

[31] Radich, E.J., Dwyer, R., Kamat, P.V. (2011). Cu_2S Reduced Graphene Oxide Composite for High-Efficiency Quantum Dot Solar Cells: Overcoming the Redox Limitations of S^{2-}/S_n^{2-} at the Counter Electrode. *Journal of Physical Chemistry Letters*, 2(19), 2453–2460. DOI: 10.1021/jz201064k.

[32] Lin, J.-Y., Chan, C.-Y., Chou, S.-W. (2013). Electrophoretic Deposition of Transparent MoS_2–Graphene Nanosheet Composite Films as Counter Electrodes in Dye-Sensitized Solar Cells. *Chemical Communications*, 49(14), 1440–1442. DOI: 10.1039/C3CC39632G.

[33] Yuan, B., Gao, Q., Zhang, X., Duan, L., Chen, L., Mao, Z., Li, X., Lü, W. (2018). Reduced Graphene Oxide (RGO)/Cu_2S Composite as Catalytic Counter Electrode for Quantum Dot-Sensitized Solar Cells. *Electrochimica Acta*, 277, 50–58. DOI: 10.1016/j.electacta.2018.04.218.

[34] Akman, E., Altıntas, Y., Gulen, M., Yilmaz, M., Mutlugun, E., Sonmezoglu, S. (2020). Improving Performance and Stability in Quantum Dot-Sensitized Solar Cell through Single Layer Graphene/Cu_2S Nanocomposite Counter Electrode. *Renewable Energy*, 145, 2192–2200. DOI: 10.1016/j.renene.2019.07.163 .

[35] Prasad, A.K., Jo, I.R., Kang, S.H., Ahn, K.S. (2021). Novel Method for Synthesis of Reduced Graphene Oxide–Cu_2S and Its Application as a Counter Electrode in Quantum-Dot-Sensitized Solar Cells. *Applied Surface Science*, 564, 150393. DOI: 10.1016/j.apsusc.2021.150393.

[36] Nguyen, T.P., Ha, T.T., Nguyen, T.T., Ho, N.P., Huynh, T.D.; Lam, Q.V. (2018). Effect of Cu^{2+} Ions Doped on the Photovoltaic Features of CdSe Quantum Dot Sensitized Solar Cells. *Electrochimica Acta*, 282(1), 16–23. DOI: 10.1016/j.electacta.2018.06.046.